AAS 25-621

STABLE, LOW-ENERGY PROGRADE EARTH-MOON CYCLER ORBITS

Shane D. Ross* **and Michael Roberts-Tsoukkas†**

We present a new class of low-energy, prograde Earth-Moon cycler orbits; natural periodic trajectories that alternately orbit the Earth and Moon, without requiring propulsion. Unlike previously studied cycler orbits, these orbits are fully ballistic, prograde, and include stable orbits. Their geometry enables potential use in space situational awareness, communications, search-and-rescue, and infrastructure development. A systematic method is introduced to design families of these cyclers with specified Earth and Moon orbit counts, revealing resonant and highly maneuverable regimes that offer new opportunities for cislunar mission design.

INTRODUCTION

Earth-Moon cycler orbits, sometimes called lunar cyclers, are trajectories that periodically travel between Earth and the Moon, providing a regular and efficient means of transportation for spacecraft, supplies, or potentially humans. They are particularly attractive for applications in space domain awareness (SDA), communications, position-navigation-timing (PNT), and infrastructure development, especially if deployed in constellations.

Several Earth–Moon cyclers have been developed in the literature, including the Arenstorf cyclers,[1] the Aldrin cycler,[2] and various other families.[3–9] To our knowledge, however, the orbits presented here are the first natural (i.e., ballistic) Earth–Moon cyclers that alternately encircle both the Earth and the Moon in a prograde, temporary-capture fashion and exhibit stability. Leiva and Briozzo[10,11] identified a single unstable orbit resembling one of the classes presented here, but did not identify the continuous families of unstable and stable cyclers we report.

In this work, we present a new class of low-energy, prograde Earth-Moon cycler orbits that are fully ballistic and, remarkably, include stable families. These orbits alternately encircle the Earth and the Moon in the rotating frame, repeating this pattern with fixed geometry and period. To our knowledge, this is the first demonstration of stable, prograde, natural cyclers that exhibit temporary capture around each primary.

More importantly, we develop a systematic geometric method to construct families of such orbits, characterized by the number of synodic circuits about the Earth (k_1) and the Moon (k_2). These (k_1, k_2)-cyclers form a one-parameter family with *stable sub-families*, each of which can be represented as a continuous curve in (x, C) space, where x is a perpendicular Earth-Moon line crossing and C is the Jacobi constant.[12]

Figure 1 shows representative examples of stable prograde cyclers. Their proximity to chaotic regions in phase space, demonstrated below, implies high maneuverability, and several exhibit resonance with the synodic period of the Moon. For instance, the 45-day period of the $(1, 1)$-cycler is

*Professor, Aerospace and Ocean Engineering, Virginia Tech, Blacksburg, VA, USA, sdross@vt.edu
†Undergraduate Researcher, Aerospace and Ocean Engineering, Virginia Tech, Blacksburg, VA, USA, michaelbrt@vt.edu

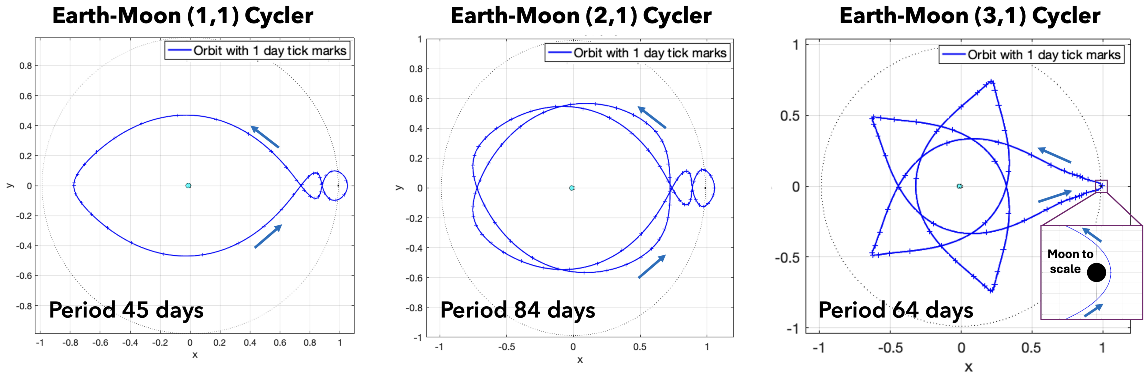

Figure 1: Examples of stable prograde Earth-Moon cyclers, shown in the Earth-Moon rotating (synodic) frame, in non-dimensional units. One day tick marks are shown. The Earth is near the origin and the Moon near 1 on the x-axis. Both bodies are shown to scale.

close to the 2:3 resonance with the Sun-Earth synodic period, yielding periodic Sun-Earth-Moon-spacecraft alignments.

This work builds upon the theoretical foundation of the Global Orbit Structure Theorem by Koon et al.,[13] which proved the existence of unstable periodic orbits near a homoclinic-heteroclinic cycle connecting the L_1 and L_2 Lyapunov orbits. While constructive, the theorem did not specify the size of the neighborhood in which it held, leaving open the possibility of stable orbits beyond its scope. We revisit a key assumption of the theorem: that the stable and unstable manifold tubes of the L_1 and L_2 Lyapunov orbits enclose all trajectories transitioning between the Earth- and Moon-dominated regions. Our results show that stable cyclers reside within this region, but beyond the reach of prior unstable constructions.

PLANAR CIRCULAR RESTRICTED THREE-BODY MODEL

The planar circular restricted three-body problem (PCR3BP) is the simplest model that captures the qualitative features of spacecraft dynamics in cislunar space.[14] It describes the motion of a massless spacecraft in a rotating frame defined by two primary bodies (e.g., Earth and Moon) that revolve in circular orbits around their barycenter. All motion is confined to the Earth-Moon plane.

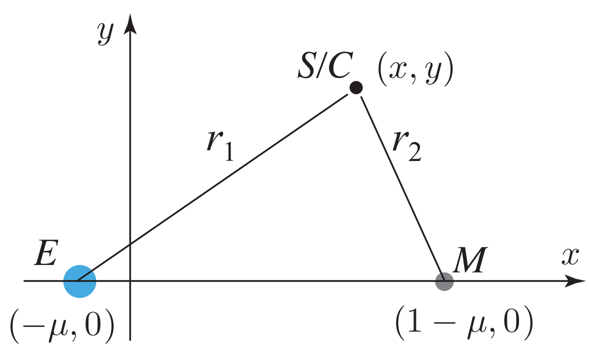

Figure 2: Geometry of the planar circular restricted three-body problem (PCR3BP) in the non-dimensional co-rotating (x, y) frame, showing Earth (E), Moon (M), & spacecraft (S/C).

We adopt normalized units: the Earth-Moon distance (i.e., average semi-major axis $a_m = 384{,}400$ km) is 1, the total mass of the primaries ($m_1 + m_2$) is 1, and the orbital period of the Earth and Moon relative to the inertial barycentric frame (the sidereal period $T_m = 27.321661$ days) is 2π. The only system parameter is the mass ratio $\mu = m_2/(m_1 + m_2)$, for which we use the Earth-Moon value,

$$\mu = 1.2150584270572 \times 10^{-2}.$$

We center the rotating frame at the barycenter, placing Earth and Moon at $(-\mu, 0)$ and $(1 - \mu, 0)$, respectively, along the x-axis. The equations of motion for the spacecraft in these units are,

$$\begin{aligned} \ddot{x} - 2\dot{y} &= -\frac{\partial \bar{U}}{\partial x} = x - (1-\mu)\frac{x+\mu}{r_1^3} - \mu\frac{x-1+\mu}{r_2^3}, \\ \ddot{y} + 2\dot{x} &= -\frac{\partial \bar{U}}{\partial y} = y - (1-\mu)\frac{y}{r_1^3} - \mu\frac{y}{r_2^3}, \end{aligned} \tag{1}$$

where the distances from the spacecraft to Earth and Moon are given by,

$$r_1 = \sqrt{(x+\mu)^2 + y^2}, \quad r_2 = \sqrt{(x-1+\mu)^2 + y^2},$$

and the effective potential function is,[15]

$$\bar{U}(x, y) = -\tfrac{1}{2}(x^2 + y^2) - \frac{1-\mu}{r_1} - \frac{\mu}{r_2}. \tag{2}$$

A point in the four-dimensional phase space $\mathcal{M}$ is denoted by $X = (x, y, \dot{x}, \dot{y})$, or alternatively by instantaneous (i.e., osculating) geocentric orbital elements $X = (a, e, \ell, g)$, where a is semi-major axis, e eccentricity, ℓ mean anomaly, and g the longitude of perigee relative to the rotating x-axis.

Jacobi Constant, Energy Manifolds, and Hill's Region

The Jacobi integral $\mathcal{C}$ is a conserved scalar quantity along any trajectory of the PCR3BP equations (1),

$$\mathcal{C}(x, y, \dot{x}, \dot{y}) \equiv -2\bar{U}(x, y) - (\dot{x}^2 + \dot{y}^2). \tag{3}$$

We follow the convention in the cislunar astrodynamics community, omitting the additive constant $\mu(1 - \mu)$ used by some authors to normalize $C(L_4) = C(L_5) = 3$.

Each constant-$\mathcal{C}$ trajectory lies on a three-dimensional energy surface $\mathcal{M}_C$ embedded in $\mathcal{M}$,

$$\mathcal{M}_C = \mathcal{C}^{-1}(C) \equiv \{X \in \mathcal{M} \mid \mathcal{C}(X) = C\}. \tag{4}$$

The projection of this surface onto the configuration space (x, y) defines the Hill's region,

$$H_C = \{(x, y) \mid x^2 + y^2 + 2\left((1-\mu)/r_1 + \mu/r_2\right) \geq C\}. \tag{5}$$

with boundary ∂H_C called the zero-velocity curve, where $\dot{x} = \dot{y} = 0$. For natural (i.e., propulsion-less) trajectories, the spacecraft is restricted to remain within H_C.

There are five distinct Hill's region topologies, depending on C. Our interest is primarily in cases 2 and 3 (see Figure 3). In case 2 ($C_1 > C > C_2$), a bottleneck opens at L_1, allowing Earth–Moon transitions. In case 3 ($C_2 > C > C_3$), an additional bottleneck opens at L_2, permitting transitions to the exterior realm.

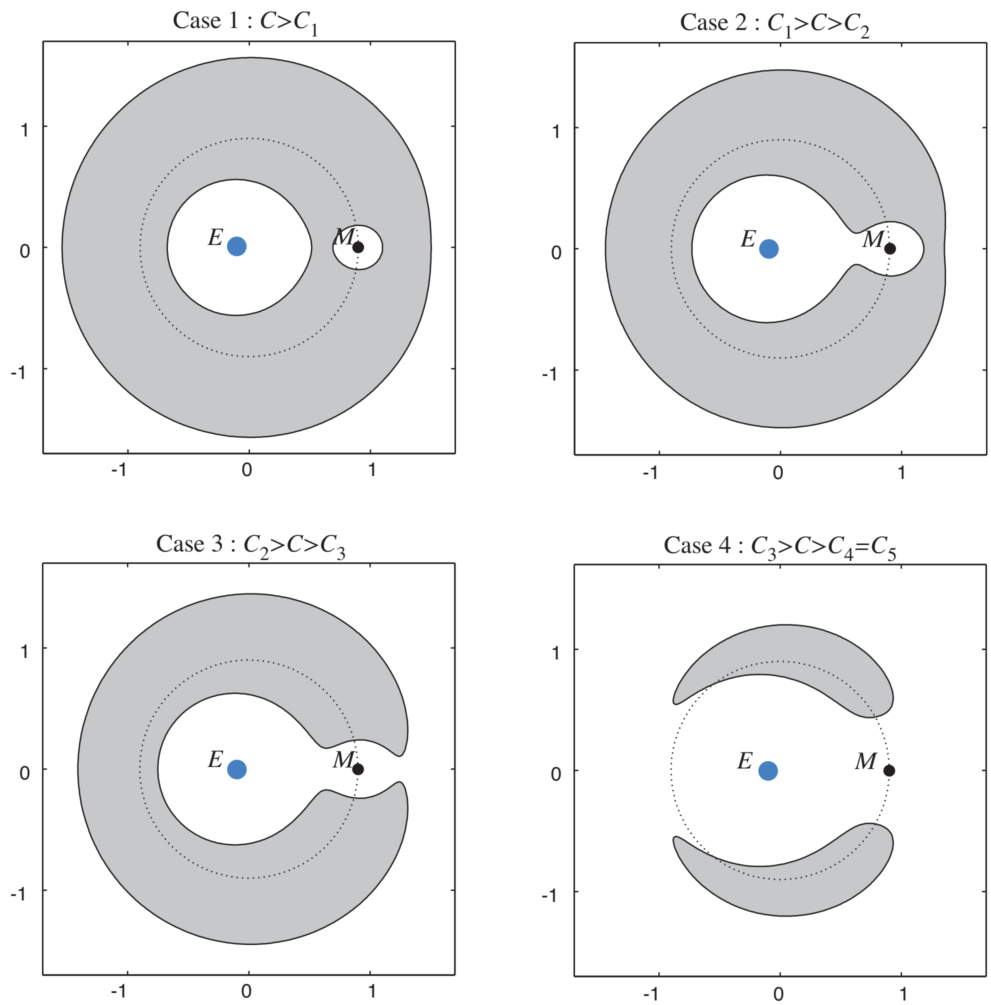

Figure 3: Four cases of the Hill's regions H_C in the Earth-Moon rotating (synodic) frame, illustrating changes in admissible motion as the Jacobi constant C varies.

The shaded region outside the Hill's region is where motion is inadmissible due to the Jacobi constant constraint, sometimes denoted the *forbidden realm*. The small oval region on the right is the *Moon realm*, consisting largely (but not entirely) of selenocentric orbits (Moon is the dominant mass). The large near-circular region on the left is the *Earth realm* surrounding the Earth, consisting largely of geocentric orbits (Earth is the dominant mass). The region which lies outside the shaded forbidden region is the *exterior realm* surrounding the Earth (and Moon), and also largely consists of geocentric orbits (Earth is the dominant mass).

The values of C which separate these five cases are denoted $C_i, i = 1, 2, 3, 4$ which are the values corresponding to the equilibrium points, $C_i = C(L_i)$; note $C_4 = C_5$. For case 2, where the Jacobi constant lies between C_1 and C_2, a bottleneck is open around the Lagrange point L_1, and spacecraft orbits going between the Earth realm and Moon realm are energetically possible. For case 3, the Hill's region contains a neck around both L_1 and L_2 and the spacecraft can transit from the Earth realm to the exterior realm and vice versa.

POINCARÉ SURFACES OF SECTION AND CYCLER CLASSIFICATION

To characterize Earth-Moon cyclers, we define four Poincaré sections in the rotating frame,

$U_1^- = \{(x, \dot{x}) \mid y = 0,\ x < -\mu,\ \dot{y}(x, \dot{x}; C) < 0\}$, in the E realm;

$U_1^+ = \{(x, \dot{x}) \mid y = 0,\ x > -\mu,\ \dot{y}(x, \dot{x}; C) > 0\}$, in the E realm;

$U_2^- = \{(x, \dot{x}) \mid y = 0,\ x < 1-\mu,\ \dot{y}(x, \dot{x}; C) < 0\}$, in the M realm,

$U_2^+ = \{(x, \dot{x}) \mid y = 0,\ x > 1-\mu,\ \dot{y}(x, \dot{x}; C) > 0\}$, in the M realm,

where $\dot{y}(x, \dot{x}; C)$ denotes that $\dot{y}$ is obtained from the Jacobi constant equation (3). See Figure 4. We also define $U_1 = U_1^- \cup U_1^+$ and $U_2 = U_2^- \cup U_2^+$.

Definition of (k_1, k_2)-Cyclers

We define a periodic (prograde) Earth-Moon cycler by the number of times it crosses the sections U_1^- and U_2^+ during each cycle.

Definition 1. *A* (k_1, k_2)-cycler *is a periodic solution of* (1) *that crosses section* U_1^- *exactly* k_1 *times and section* U_2^+ *exactly* k_2 *times before repeating. Here,* $k_1, k_2 \in \mathbb{Z}^+$.

For instance, the trajectories shown in Figure 1 are $(k_1, 1)$-cyclers for $k_1 = 1, 2, 3$. The definitions of U_1^- and U_2^+ ensure that these crossings correspond to prograde motion: U_1^- selects Earth-bound crossings with $\dot{y} < 0$, and U_2^+ selects Moon-bound crossings with $\dot{y} > 0$.

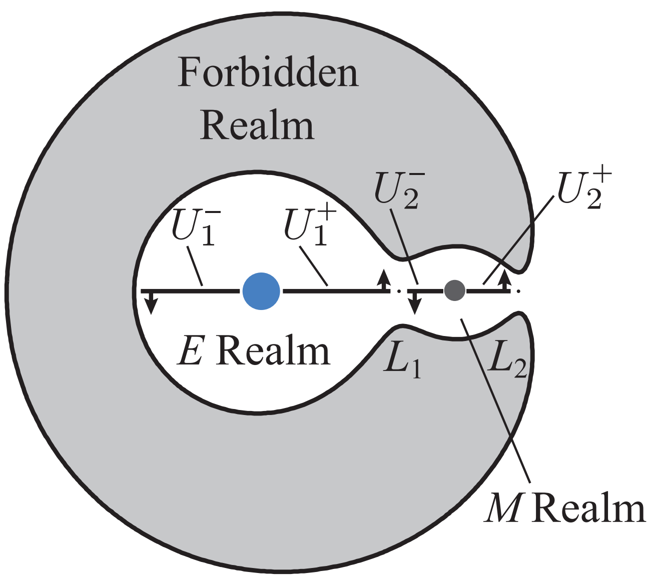

Figure 4: Location of the four Poincaré sections in the Earth (E) and Moon (M) realms. Arrows indicate the sign of $\dot{y}$, i.e., ascending or descending crossing. L_1 and L_2 are shown for reference.

MANIFOLD TUBES

For each Jacobi constant $C < C_1$, there exists a unique planar Lyapunov periodic orbit about the L_1 libration point. This orbit is of saddle type and thus possesses both stable and unstable two-dimensional invariant manifolds with cylindrical geometry, denoted $W^s_{L_1,\text{p.o.}}$ and $W^u_{L_1,\text{p.o.}}$, respectively.

Each of these manifolds has two branches: one extending toward the Earth realm and one toward the Moon realm. We indicate these using an additional superscript, e.g., $W^{s,E}_{L_1,\text{p.o.}}$ and $W^{s,M}_{L_1,\text{p.o.}}$. These manifolds serve as *co-dimension-one separatrices* within the constant energy surface $\mathcal{M}_C$, partitioning transit and non-transit trajectories.

As an example, we label by $T_{M,[E]}$ the three-dimensional solid tube of trajectories currently in the Earth realm that originated in the Moon realm, bounded by the cylindrical surface $W^{u,E}_{L_1,\text{p.o.}}$. This unstable manifold surface is therefore the boundary $\partial T_{M,[E]}$.

Trajectories inside these tubes execute transit orbits: either $T_{[E],M} \cup T_{E,[M]}$ (Earth-to-Moon) or their time-reversed counterparts $T_{[M],E} \cup T_{M,[E]}$ (Moon-to-Earth). Figure 5 illustrates the geometry of the L_1 manifold tubes as projected onto configuration space, up to their first intersection with the Poincaré sections U_1^- and U_2^+.

Manifold Tube Intersections: Tube Dynamics

To construct Earth-Moon cyclers with a specific number of Earth realm crossings, $k_1 = 1$, we seek an overlap of the interior of the stable and unstable manifold branches $W^{s,E}_{L_1,\text{p.o.}}$ and $W^{u,E}_{L_1,\text{p.o.}}$; i.e., the intersection $T_{[E],M} \cap T_{E,[M]}$ on the Poincaré section U_1^-. This intersection only exists if the first cuts of both manifolds on U_1^- overlap; otherwise, only cyclers with $k_1 \geq 2$ are possible.

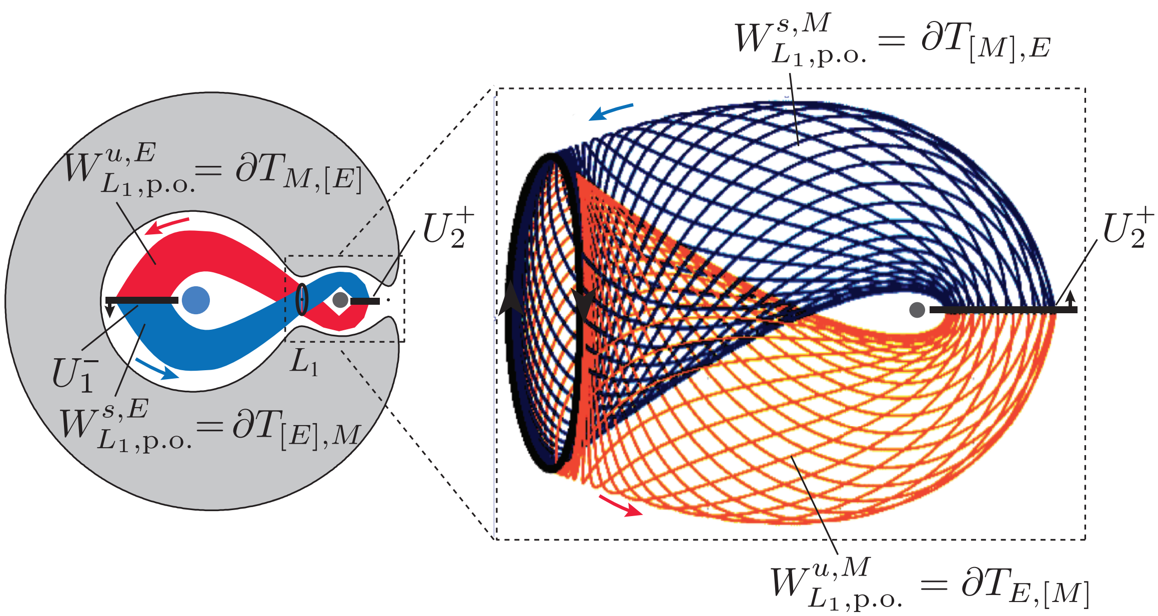

Figure 5: Projection of the L_1 periodic orbit manifold tubes onto configuration space, connecting the Poincaré sections U_1^- and U_2^+. The energy considered is in the case 3 regime (see Figure 3).

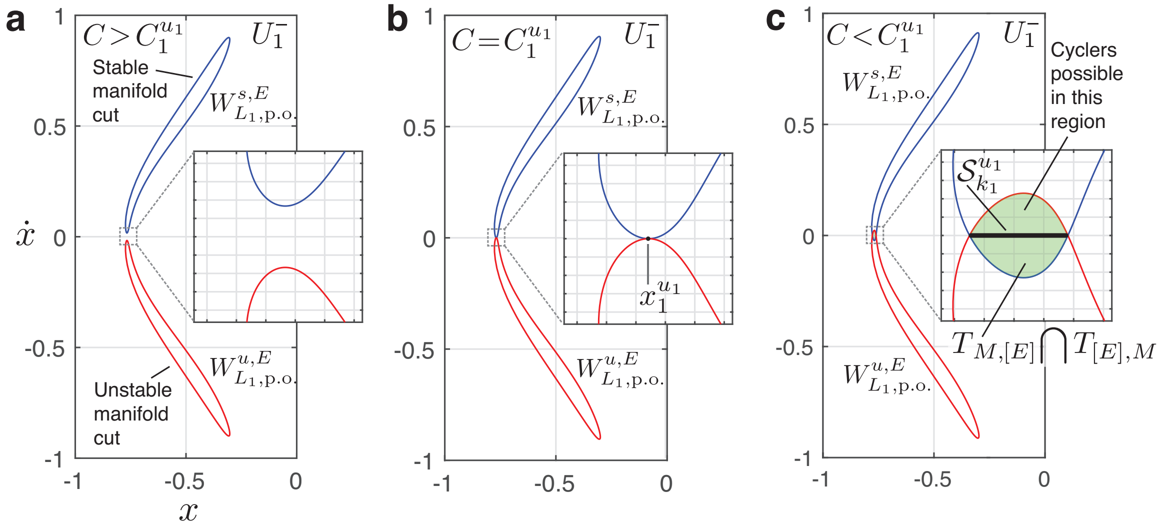

Figure 6: Identification of the critical Jacobi constant $C_1^{u_1}$ for the emergence of $k_1 = 1$ symmetric cyclers. (a) Manifolds do not overlap. (b) Tangency occurs at $x_1^{u_1} \approx -0.768$. (c) For $C < C_1^{u_1}$, initial conditions which correspond to Earth-Moon $(1, k_2)$-cyclers, if they exist, must be within the shaded region, the intersection of the interior of $W^{u,E}_{L_1,\text{p.o.}}$ and $W^{s,E}_{L_1,\text{p.o.}}$. Symmetric cyclers will be in the subset $\mathcal{S}^{u_1}_{k_1}$, the thick line along $\{\dot{x} = 0\}$.

As C decreases further below C_1, the manifold cross-sectional areas on U_1 increase approximately proportionally to $\Delta C = C_1 - C$ for small ΔC.[16] At a critical Jacobi constant $C_1^{u_1}$, the first cuts become tangent along the symmetry line $\{\dot{x} = 0\}$, at a location denoted $x_1^{u_1}$. This tangency marks the first possible emergence of symmetric $(1, k_2)$-cyclers. See the sequence near this tangency in Figure 6. Note that due to the time-reversal symmetry of the equations of motion, the stable and unstable manifolds appear as symmetric about the line $\{\dot{x} = 0\}$.

For $C < C_1^{u_1}$, the shaded intersection region in Figure 6(c) contains initial conditions where $k_1 = 1$ cyclers are theoretically possible. All initial conditions in this shaded region of the Poincaré section are such that when numerically integrated backward in time they transit to the M realm, and when integrated forward in time, they also transit to the M realm.

Symmetric Cyclers

To simplify the analysis, we restrict attention to symmetric cyclers; those with initial conditions along the line $\{\dot{x} = 0\}$. For general k_1, we define the corresponding symmetry-reduced subset of U_1 as $\mathcal{S}^{u_1}_{k_1}$,

$$\mathcal{S}^{u_1}_{k_1} \equiv U_1 \cap \{\dot{x} = 0\} \cap \text{int}(W^{s,E(k_1)}_{L_1,\text{p.o.}}) \cap \text{int}(W^{u,E(k_1)}_{L_1,\text{p.o.}}), \tag{6}$$

where $W^{s,E(n)}_{L_1,\text{p.o.}}$ denotes the n-th cut of the stable manifold with U_2, and $W^{u,E(n)}_{L_1,\text{p.o.}}$ denotes the n-th cut of the unstable manifold with U_2. Note that $\mathcal{S}^{u_1}_{k_1}$ could be disconnected set.

Even for $C > C_1^{u_1}$, such intersections may still exist, but only after several revolutions ($k_1 \geq 2$) around the Earth. We compute the Jacobi constant $C^{u_1}_{k_1}$ and intersection point $x^{u_1}_{k_1}$ for up to three U_1^- crossings, tabulated in Table 1.

A parallel construction applies for the Moon side, using the M-branches of the L_1 manifold tubes

Table 1: Jacobi constants and x-locations where cyclers with k_1 crossings of the U_1^- Poincaré section.

k_1	$C_{k_1}^{u_1}$	$x_{k_1}^{u_1}$
1	3.151763728314920	−0.767856324800
2	3.129751730201047	0.723754610150
3	3.188341092440989	−0.332153924455

and the Poincaré section U_2. We define the Moon-side symmetry-reduced region for k_2 crossings as,

$$\mathcal{S}_{k_2}^{u_2} \equiv U_2 \cap \{\dot{x} = 0\} \cap \mathrm{int}(W_{L_1,\text{p.o.}}^{s,M(k_2)}) \cap \mathrm{int}(W_{L_1,\text{p.o.}}^{u,M(k_2)}), \tag{7}$$

where $W_{L_1,\text{p.o.}}^{s,M(n)}$ denotes the n-th cut of the stable manifold with U_2, etc. The corresponding values of $(C_{k_2}^{u_2}, x_{k_2}^{u_2})$ are given in Table 2.

For categorization, we count the number of crossings of U_1^-. But for symmetric cyclers, the Earth realm *perpendicular* crossings can occur on either U_1^- or U_1^+. Similarly, we count the number of crossings of U_2^+, but the Moon realm perpendicular crossings can occur on either U_2^- or U_2^+. In Broucke (1968)'s symmetric orbit classification,[12] the orbits we identify correspond to classes 2, 3, or 5, depending on their crossings.

Table 2: Jacobi constants and x-locations for symmetric cyclers with k_2 crossings of the U_2^+ Poincaré section.

k_2	$C_{k_2}^{u_2}$	$x_{k_2}^{u_2}$
1	3.1833333078762	1.0016252150
2	3.1840565764573	0.8611415325
3	3.1845534633380	1.0110341410

Interestingly, while $C_{k_2}^{u_2}$ increases monotonically with k_2, the Earth-side bounds $C_{k_1}^{u_1}$ are not monotonic.

GENERATING SYMMETRIC PERIODIC EARTH-MOON CYCLERS

The value $C_{k_1}^{u_1}$ is where the L_1 Lyapunov orbit's stable and unstable manifolds—Earth realm branch—first intersect along the section U_1, tangential to the line $\{\dot{x} = 0\}$ (see Figure 6b). Similarly, $C_{k_2}^{u_2}$ is the corresponding intersection value for the Moon realm branch along section U_2.

For a given (k_1, k_2), the theoretical upper bound Jacobi constant for a symmetric (k_1, k_2)-cycler is,

$$C_{(k_1,k_2)} \equiv \min \left\{ C_{k_1}^{u_1}, C_{k_2}^{u_2} \right\}. \tag{8}$$

For $C < C_{(k_1,k_2)}$, we take the set $\mathcal{S}_{k_1}^{u_1} \subset U_1$ and flow it forward under the PCR3BP dynamics until it intersects $\mathcal{S}_{k_2}^{u_2} \subset U_2$. Let this map be denoted P. The set

$$\Gamma^{u_2} \equiv P(\mathcal{S}_{k_1}^{u_1}) \cap \mathcal{S}_{k_2}^{u_2}$$

will be at most a discrete set of points, which correspond to initial conditions along symmetric (k_1, k_2)-cyclers. Each such point is flowed back to U_1 to define $\Gamma^{u_1} = P^{-1}(\Gamma^{u_2})$. Given the numerical discretization of Γ^{u_1}, we apply differential correction to refine approximate initial conditions into a true cycler periodic orbit; one that closes within a specified tolerance.

Differential Correction (Fixed Jacobi Constant)

Let $x_0^g \in \Gamma^{u_1}$ be an initial guess. To satisfy the fixed Jacobi constant C, we determine $\dot{y}_0^g$ from,

$$\mathcal{C}(x_0^g, 0, 0, \dot{y}_0^g) = C. \tag{9}$$

By the implicit function theorem, we will refer to $\dot{y}_0^g$ as a function of x_0^g and C, denoted $\dot{y}_0^g(x_0^g, C)$.

We exploit the time-reversal symmetry about the x-axis,

$$s_x : (x, y, \dot{x}, \dot{y}, t) \to (x, -y, -\dot{x}, \dot{y}, -t), \tag{10}$$

to ensure periodicity. Because cyclers are symmetric, their midpoint also lies on the x-axis with $\dot{x} = 0$.

Starting from $t = 0$, we integrate our initial guess forward to the first crossing of the neighborhood of $\mathcal{S}_{k_2}^{u_2}$ at time t_1. To ensure symmetry, we require a perpendicular x-axis crossing,

$$y(t_1) = 0, \quad \dot{x}(t_1) = 0. \tag{11}$$

This reduces the boundary-value problem to a single unknown, x_0. We apply Newton–Raphson iterations to correct x_0, updating $\dot{y}_0$ to maintain C, until $|\dot{x}(t_1)| < \varepsilon$ for a small tolerance $\varepsilon \ll 1$.

The differential correction loop is as follows.[17]

1. **Integrate to half-period.** From the current (suppose the n-th) guess $(x_0^g(n), 0, 0, \dot{y}_0^g(n))$, integrate both the trajectory and state transition matrix $\Phi(t_1, 0)$ to the first intersection with the neighborhood of $\mathcal{S}_{k_2}^{u_2}$. Record the crossing t_1, state at crossing $(x_1, y_1, \dot{x}_1, \dot{y}_1)$, and matrix $\Phi(t_1, 0)$, with entries Φ_{ij}.

2. **Check symmetry.** If $|\dot{x}_1| < \varepsilon$, stop.

3. **Compute correction.** From differential correction[15] and the constraint to keep the Jacobi integral (3) constant, compute the update δx_0 needed to remove $\dot{x}_1$,

$$\delta x_0 = \dot{x}_1 \left(\frac{\dot{y}_1}{\ddot{x}_1 \, \Phi_{21}} \right) \left[1 - \frac{\Phi_{24}}{\Phi_{21}} \frac{1}{\dot{y}_0^g(n)} \frac{\partial \bar{U}}{\partial x}(0) - \frac{\dot{y}_1}{\ddot{x}_1} \frac{1}{\Phi_{21}} \left(\Phi_{31} - \Phi_{34} \frac{1}{\dot{y}_0^g(n)} \frac{\partial \bar{U}}{\partial x}(0) \right) \right]^{-1}, \tag{12}$$

   where $\ddot{x}_1$ is computed via the equations of motion (1), and $\partial \bar{U}/\partial x(0)$ is evaluated at the initial location.

4. **Update guess.** Apply the correction and re-enforce the Jacobi constant, to obtain the $(n+1)$-th guess from the n-th guess,

$$x_0^g(n+1) = x_0^g(n) + \delta x_0, \qquad \dot{y}_0^g(n+1) \; = \; \pm\sqrt{-\,2\,\bar{U}\big(x_0^g(n+1), 0\big) \; - \; C}\,.$$

   Here the sign in $\dot{y}_0^g(n+1)$ is chosen appropriate for $\mathcal{S}_{k_2}^{u_2}$. Return to Step 1.

With $\varepsilon = 10^{-8}$ (about 10^{-5} m/s), convergence is typically reached within $n = 5$ iterations, and we then have a periodic cycler orbit of period $T = 2t_1$ with initial x-value x_0 along the x-axis with the targeted Jacobi constant C.

Stability of Cycler Periodic Orbits

Stability is determined by the monodromy matrix, $M = \Phi(T, 0)$, the state transition matrix after one period. Since this is a symmetric orbit, we can obtain M from the last calculated state transition matrix for the half-period, $\Phi(T/2, 0)$, from the algorithm above, since $t_1 = T/2$. This is more efficient and reduces errors due to numerical integration. As a property of state transition matrices, we have,

$$M = \Phi(T, 0) = \Phi(T, T/2)\Phi(T/2, 0), \tag{13}$$

where, using a result from Barden (1994)[18] for symmetric periodic orbits*, we have,

$$\Phi(T, T/2) = G\Phi(T/2, 0)^{-1}G, \tag{14}$$

where $G = \mathrm{diag}(1, -1, -1, 1)$ encodes the s_x symmetry (10).

Since the PCR3BP is a Hamiltonian system, M has a double eigenvalue 1, and determinant of 1, and the stability is determined by the remaining two eigenvalues,[15,20] which have the form λ and $1/\lambda$. We measure stability with the *stability parameter*[21,22] which we define as,

$$\nu = \tfrac{1}{2}(\lambda + 1/\lambda). \tag{15}$$

The orbit is linearly stable if $|\nu| < 1$, and unstable otherwise. We note that when $\nu \leq -1$ or $\nu \geq 1$, both λ and $1/\lambda$ are real, and when $-1 < \nu < 1$, λ and $1/\lambda = \bar{\lambda}$ are complex conjugates on the unit circle.

Generating Cycler Families via Continuation

When one periodic orbit is found on a given energy manifold $\mathcal{M}_C$, the theory of Hamiltonian systems guarantees the existence of a continuous one-parameter family of periodic orbits nearby.[15]

Let $(x(0), C(0))$ denote the initial solution in a cycler family, parameterized by an arc-length variable s. Then the full family $\mathcal{F}(k_1, k_2)$ can be represented as a parametric curve in (x, C) space,

$$\mathcal{F}(k_1, k_2) \equiv \{(x(s), C(s)) \mid s \in [s_{\min}, s_{\max}]\}\,. \tag{16}$$

To compute the one-parameter family of (k_1, k_2)-cycler orbits, we apply pseudo arc-length continuation[23,24] in combination with the differential correction method described above. This approach allows us to systematically trace the family of symmetric (k_1, k_2)-cyclers while simultaneously monitoring their stability.

Note that the endpoints of the family, $s_{\min}$ and $s_{\max}$, may correspond to physically inadmissible solutions, such as orbits that collide with the Moon's surface. We take the Moon's radius to be $R_m = 1{,}740$ km.

COMPUTED CYCLER FAMILIES

Using the procedures described above, we compute symmetric (k_1, k_2)-cycler families for several combinations of k_1 and k_2, as shown in Table 3. For each family, we report several values of the Jacobi constant, beginning with the theoretical upper bound $C_{(k_1,k_2)}$ from (8). The value $C^{\max}_{(k_1,k_2)}$ denotes the maximum Jacobi constant at which the cycler family first emerges; by construction, $C^{\max}_{(k_1,k_2)} < C_{(k_1,k_2)}$. Additionally, $C_{(k_1,k_2)}$ is bounded above by C_1, so $C_{(k_1,k_2)} < C_1$. The midpoint

*Based on an earlier result of Yakubovich and Starzhinskii (1975)[19]

Table 3: Earth-Moon prograde (k_1, k_2)-cycler periodic orbits.

k_1	k_2	$C_{(k_1,k_2)}$	$C^{\max}_{(k_1,k_2)}$	$C^{s}_{(k_1,k_2)}$	$T^{\text{stable}}_{(k_1,k_2)}$	Δp_m (km)
1	1	3.1517637283600	3.151175879916394	3.151175879508174	10.29206921007976	0.13
2	1	3.1297495000000	3.129389531092325	3.129389531088256	19.44043166795154	4.23
3	1	3.1833333078762	3.161796247265416	3.161784147013429	14.78849241668140	253.70
3	2	3.1840565764573	3.182762785398336	3.182762663084288	17.90058010350006	42.08
3	3	3.1845534633380	3.183379082936385	3.177224018696528	18.14546057589189	2041.34

of the largest stable sub-family—where the stability parameter $\nu = 0$ (corresponding to $\lambda = \pm i$)—is denoted $C^{\text{stable}}_{(k_1,k_2)}$ and satisfies $C^{\text{stable}}_{(k_1,k_2)} < C^{\max}_{(k_1,k_2)}$. The associated period of this representative stable orbit is $T^{\text{stable}}_{(k_1,k_2)}$, and the 'size' of the largest stable subfamily is given by the range of perilune distances, Δp_m, in kilometers (using the length scale $a_m = 384{,}400$ km). The basin of stability for each periodic orbit can be approximated by the width, in perilune altitude, of the largest surrounding resonant torus. However, this quantity is reported only for the (3,1)-cyclers.

(1,1)-Cyclers

The stable sub-family of $(1, 1)$-cyclers is extremely narrow, with a perilune width of only about 0.1 km. Notably, the midpoint of this stable sub-family (illustrated in Figure 1) has a period $T^{\text{stable}}_{(1,1)}$ of 44.7538 days. This is within 1% of the 2:3 Earth–Moon synodic resonance, where the synodic period of the Moon (full moon to full moon) is 29.530588 days. Such near-commensurability implies a nearly repeating Earth–Moon geometry, which may be advantageous for certain mission architectures.

(2,1)-Cyclers

The stable sub-family of $(2, 1)$-cyclers is slightly wider than that of the $(1, 1)$-cyclers, though still relatively narrow. A representative orbit is shown in Figure 7, depicted in both the rotating frame, where it appears as a closed loop, and the Earth-centered inertial frame, where it does not. This is because the stable period $T^{\text{stable}}_{(2,1)}$ is not an integer multiple of 2π, but approximately $3.09 \times 2\pi$.

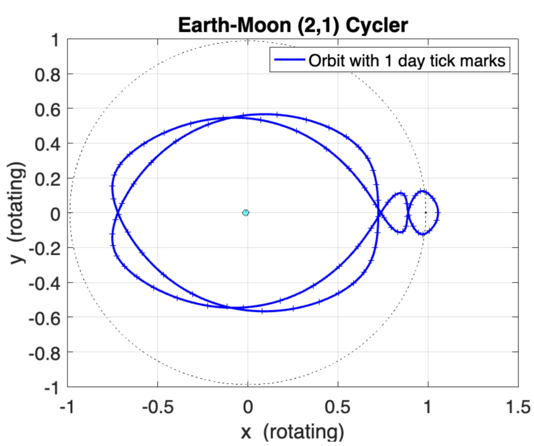

a

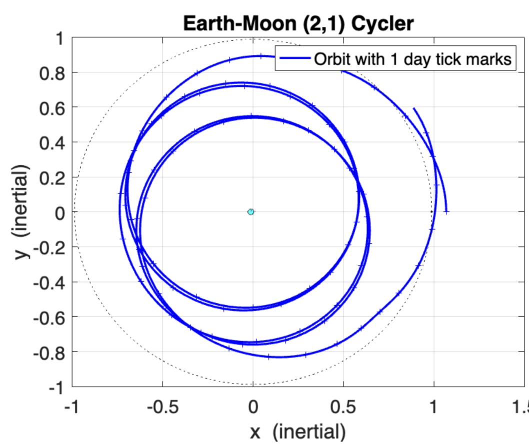

b

Figure 7: The stable (2,1)-cycler seen (a) in the rotating frame and (b) in the inertial frame.

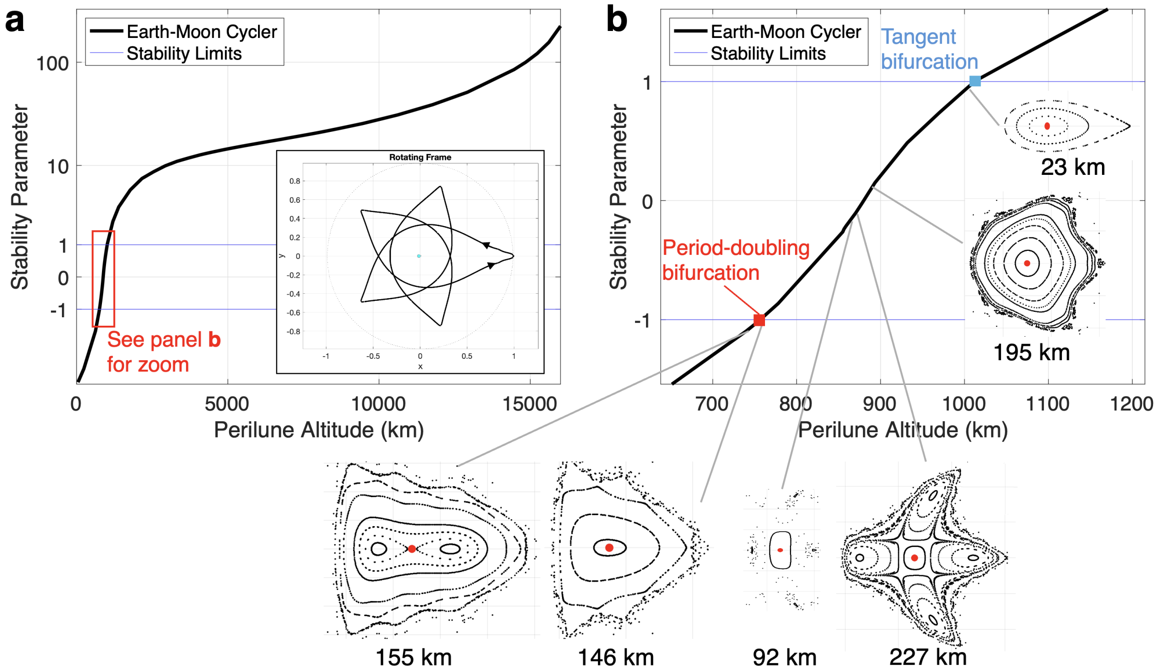

Figure 8: (a) The family of (3,1)-cyclers parameterized by perilune distance. Notice there is a stable window between perilune distances of about 750 km to 1000 km. All orbits look like the inset, which is the same as in Figure 1. (b) A zoom-in on the stable window is shown, as well as local Poincaré sections on U_2 for a sampling of orbits, showing the surrounding resonant tori, with an estimate (in km) of the size of the 'basin of stability' given by the width of the largest torus, beyond which is a chaotic region. Two bifurcations are labeled at the points where the family enters the stable window. More bifurcations are visible in the Poincaré sections.

(3,1)-Cyclers

Figure 8 illustrates the stability characteristics of the (3,1)-cycler family, parameterized by perilune altitude, from 0 km (lunar surface) to over 15,000 km. Panel (a) reveals a prominent stability window spanning perilune altitudes from approximately 750 km to 1,000 km. Within this interval, the cycler orbits exhibit a consistent spatial structure, represented by the trajectory shown in the inset, also featured in Figure 1.

Panel (b) provides a detailed view of the stable window, including local Poincaré sections on the U_2 surface (near the Moon) for several representative cyclers. These sections display well-defined resonant tori that enclose the stable periodic orbits. The numerical values beneath each Poincaré inset plot indicate the estimated width (in km) of the corresponding basin of stability, defined as the largest torus extent before the onset of chaotic motion. The bottom left Poincaré section reveals that even when the orbit in question is outside the window of stability, and thus *linearly* unstable, it may have *global stability properties*, such as being surrounded by a stable torus.

Two primary bifurcation points are marked, delineating the entry and exit of the family into the stable window. Additional bifurcations, indicative of further subtle dynamical transitions within the stable window, are also discernible in the provided Poincaré sections. Notably, several of these correspond to classical branching ratios of 1/4 and 1/2, as described by Greene's criterion for the breakup of invariant tori.[25]

Table 4: Earth-Moon prograde $(k_1, 1)$-cycler periodic orbits.

k_1	$\Delta C_{(k_1,1)}$	$\Delta C^{\text{max}}_{(k_1,1)}$	$\Delta C^{\text{stable}}_{(k_1,1)}$	$T^{\text{stable}}_{(k_1,1)}$ (TU)	$T^{\text{stable}}_{(k_1,1)}$ (days)	Δp_m (km)
1	3.657738e-02	5.878484e-04	4.082197e-10	10.292069	44.753800	0.13
2	5.859161e-02	3.599689e-04	4.069189e-12	19.440432	84.534335	4.23
3	1.272710e-02	1.381776e-02	1.210025e-05	14.788492	64.305944	253.70

$(k_1$,1)-Cyclers

A summary of the parameters for the Earth-Moon $(k_1, 1)$-cyclers is provided in Table 4. These cyclers, described above, are also shown in Figure 1. The following positive quantities are defined for convenience,

$$\Delta C_{(k_1,1)} \equiv C_1 - C_{(k_1,1)}, \quad \Delta C^{\text{max}}_{(k_1,1)} \equiv C_{(k_1,1)} - C^{\text{max}}_{(k_1,1)}, \quad \Delta C^{\text{stable}}_{(k_1,1)} \equiv C^{\text{max}}_{(k_1,1)} - C^{\text{stable}}_{(k_1,1)}. \tag{17}$$

All $(k_1, 1)$-cyclers necessarily have Jacobi constants less than $C_1 = 3.188341105401253$. In fact, for the examples presented here, they also satisfy $C_{(k_1,1)} < C_2 = 3.172160450399808$, but remain greater than C_3. This places them within the energy regime where escape from the Earth-Moon system is energetically possible, corresponding to Case 3 in Figure 3.

(3,2)-Cyclers

The (3,2)-cycler family features two distinct windows of stability. The larger of these spans approximately 40 km in perilune altitude, as shown in Figure 9. Panel (a) illustrates the variation of the stability parameter across the family, marking the stable regions, while panel (b) shows a representative orbit from the broader stable window. Interestingly, the period of these stable orbits closely matches the 2:5 Earth-Moon synodic resonance. In fact, this resonance is satisfied exactly by two nearby unstable family members, which exhibit stability indices on the order of 10 to 100. This family is also notable in that a member orbit was previously identified by Leiva and Brizzolara,[11] who demonstrated that a perturbed version of the orbit persists even under solar perturbation.

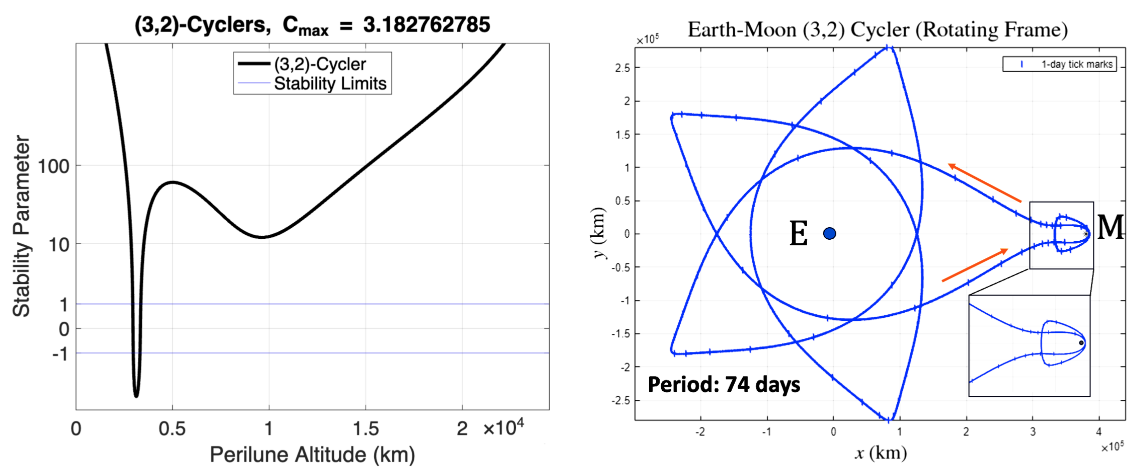

a b

Figure 9: The (3,2)-cycler family, showing (a) stability parameter vs. perilune altitude and (b) a representative orbit from a stable sub-family, shown in the rotating frame in units of km.

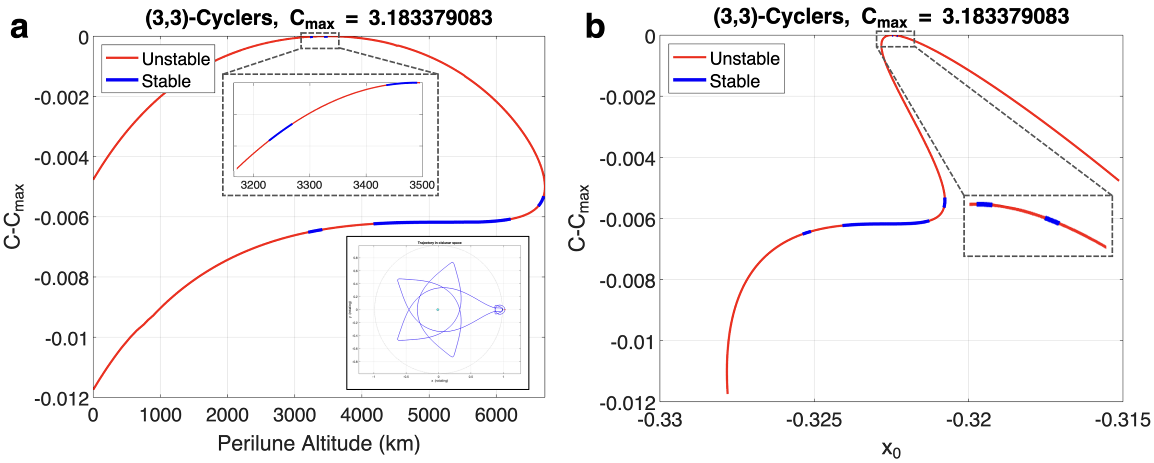

Figure 10: (a) The family of (3,3)-cyclers parameterized by perilune distance and Jacobi constant. Notice there are five stable windows. All orbits look very similar to the bottom right inset. (b) Another representation of the family in terms of the initial x condition and Jacobi constant. The non-dimensional x_0 value corresponds to perigee, and is along U_1^-.

(3,3)-Cyclers

The (3,3)-cycler family exhibits five distinct stability windows. The largest of these spans perilune altitudes from approximately 4,200 km to 6,200 km, as shown in Figure 10(a), which correspond to perigee altitudes of about 112,400 km to 113,500 km (about 3$\times$ the distance of geosynchronous orbit). The family terminates at both ends in collision with the lunar surface. Two smaller stable windows appear near $C^{\max}_{(3,3)}$, and highlighted in insets. In fact, for all (k_1, k_2)-cycler families examined, we observe a stable region near $C^{\max}_{(k_1,k_2)}$, likely due to the generic bifurcation structure that gives rise to such periodic orbits.[26]

CONCLUSION

We have presented a new class of fully ballistic, prograde Earth-Moon cycler orbits that repeatedly encircle both the Earth and Moon with episodes of temporary capture. These orbits form discrete families parameterized by the number of circuits around each body in the rotating frame and include large, previously unreported stable subfamilies.

A key contribution is not only their discovery, but also the development of a systematic geometric construction method—based on intersecting tubes of transit orbits—to initialize differential correction and continuation, a step not previously demonstrated for Earth-Moon cyclers.

We explored several, but certainly not all, (k_1, k_2)-cycler families, identifying stable subfamilies with far-side perilune altitudes ranging from 750 km to over 6,000 km. For these stable orbits, we demonstrated that their basins of stability can be approximated by the perilune width of the largest surrounding resonant torus. Anecdotally, we find that the basin width is comparable to the width of the stable subfamily itself, a relationship we intend to investigate further.

Our results reveal multiple families of periodic orbits exhibiting distinct windows of linear stability, intricate resonance structures, and rich bifurcation behavior. Notably, stable cyclers near synodic resonance conditions such as 2:3 and 2:5 synodic ratios—as seen in the (1,1) and (3,2) families, respectively—highlighting their potential for repeatable Sun-Earth-Moon geometries in mission design. Furthermore, there is evidence that these orbits will persist under common perturbations. The (3,3)-cycler families feature five distinct stable windows, including the largest stable subfamily identified, with a perilune width exceeding 2,000 km, making them especially promising for robust operational use.

Because these cycler orbits lie near or within large chaotic zones in phase space, the domain of low-energy cislunar orbits,[27,28] they offer enhanced maneuverability (to reach other regions of cislunar space) with relatively small control inputs, making them attractive for agile mission concepts.

Given their wide range over cislunar space, these cycler orbits open new avenues for cislunar mission architectures, including constellations for cislunar space domain awareness, search-and-rescue, repeatable lunar proximity operations, navigation infrastructure, and communication relays.

Future work will extend these results to non-symmetric cyclers, three-dimensional orbit families, and models that include perturbations such as lunar eccentricity and solar gravity. Low-energy cycler development will extend to the exterior realm, meaning up to the edge of the Earth's sphere of influence, with relevance for other mission concepts such as asteroid capture.[29] Applications in spacecraft deployment, transfer planning, and long-term monitoring strategies are also anticipated, particularly those requiring agile, low-energy maneuvering. As a whole, low-energy cycler families offer a new dynamical foundation for mission architectures in the emerging cislunar space economy.

ACKNOWLEDGMENT

We thank Aaron Rosengren for providing helpful historical context and references. This research was supported by the University Consortium Research Opportunity, provided by the United States Space Force (USSF) and the Air Force Research Laboratory (AFRL) under USRA Cooperative Agreement Number FA9453-21-2-0064, for xRADAR: xGEO Robust and Adaptive Space Domain Awareness. DISTRIBUTION A. Approved for public release: distribution unlimited. Public Affairs approval AFRL-2025-3466.

REFERENCES

[1] R. F. Arenstorf, "Existence of periodic solutions passing near both masses of the restricted three-body problem," *AIAA Journal*, Vol. 1, No. 1, 1963, pp. 238–240.

[2] B. Aldrin, "Cyclic Trajectory Concepts," SAIC presentation to the Interplanetary Rapid Transit Study Meeting, Jet Propulsion Laboratory, Pasadena, CA, October 28, 1985.

[3] C. Uphoff and M. Crouch, "Lunar cycler orbits with alternating semi-monthly transfer windows," *Journal of the Astronautical Sciences*, Vol. 41, No. 2, 1993, pp. 189–205.

[4] J. Casoliva, K. Mease, J. Mondelo, B. Villac, E. Barrabes, and M. Olle, "Families of cycler trajectories in the Earth-Moon system," *AIAA/AAS Astrodynamics Specialist Conference and Exhibit*, 2008, p. 6434.

[5] J. Casoliva, J. M. Mondelo, B. F. Villac, K. D. Mease, E. Barrabes, and M. Olle, "Two classes of cycler trajectories in the Earth-Moon system," *Journal of guidance, control, and dynamics*, Vol. 33, No. 5, 2010, pp. 1623–1640.

[6] A. L. Genova and B. Aldrin, "Circumlunar Free-Return Cycler Orbits for a Manned Earth-Moon Space Station," *AAS/AIAA Astrodynamics Specialist Conference*, No. AAS 15-794, Vail, CO, August 2015.

[7] L. De Leo and M. Pontani, "Low-thrust orbit dynamics and periodic trajectories in the Earth-Moon system," *Aerotecnica Missili & Spazio*, Vol. 101, No. 2, 2022, pp. 171–183.

[8] A. P. Wilmera and R. A. Bettingerb, "Earth-Moon logistical operations utilizing Cislunar periodic orbits," *International Astronautical Congress*, No. Paper No. IAC-22-E2.2, Paris, France, 2022.

[9] M. M. Wittal, S. Miaule, and B. W. Asher, "Earth-Moon Cycler Mission Design for Lunar Logistics," *International Astronautical Congress*, No. IAC-22-C1. 6.6, Paris, France, 2022.

[10] A. Leiva and C. Briozzo, "Control of chaos and fast periodic transfer orbits in the Earth-Moon CR3BP," *Acta Astronautica*, Vol. 58, No. 8, 2006, pp. 379–386.

[11] A. M. Leiva and C. B. Briozzo, “Extension of fast periodic transfer orbits from the Earth–Moon RTBP to the Sun–Earth–Moon quasi-bicircular problem,” *Celestial Mechanics and Dynamical Astronomy*, Vol. 101, 2008, pp. 225–245.

[12] M. R. Broucke, “Periodic Orbits in the Restricted Three-Body Problem with Earth–Moon Masses,” Technical Report 32–1168, NASA, Pasadena, CA, 1968.

[13] W. S. Koon, M. W. Lo, J. E. Marsden, and S. D. Ross, “Heteroclinic connections between periodic orbits and resonance transitions in celestial mechanics,” *Chaos*, Vol. 10, 2000, pp. 427–469.

[14] K. A. Ehricke, “Cislunar Orbits,” *Orbit Theory*, Vol. 9, 1959, p. 48.

[15] W. S. Koon, M. W. Lo, J. E. Marsden, and S. D. Ross, *Dynamical Systems, the Three-Body Problem and Space Mission Design*. ISBN 978-0-615-24095-4: Marsden Books, 2022.

[16] S. D. Ross, A. E. BozorgMagham, S. Naik, and L. N. Virgin, “Experimental validation of phase space conduits of transition between potential wells,” *Physical Review E*, Vol. 98, No. 5, 2018, p. 052214.

[17] A. Braik and S. D. Ross, “Heteroclinic Transfer Between L1 and L3 in Earth-Moon System,” *AAS/AIAA Astrodynamics Specialist Conference*, No. AAS 25-716, Boston, MA, August 2025.

[18] B. T. Barden, *Using Stable Manifolds to Generate Transfers in the Circular Restricted Problem of Three Bodies*. Purdue University: M.S. Thesis, 1994.

[19] V. A. Yakubovich and V. M. Starzhinskii, *Linear Differential Equations with Periodic Coefficients*. 1975.

[20] J. E. Marsden and T. S. Ratiu, *Introduction to Mechanics and Symmetry: A Basic Exposition of Classical Mechanical Systems*, Vol. 17. Springer Science & Business Media, 2013.

[21] J. V. Breakwell and J. V. Brown, “The Halo Family of 3-Dimensional Periodic Orbits in the Earth-Moon Restricted 3-Body Problem,” *Celestial Mechanics*, Vol. 20, 1979, pp. 389–404.

[22] K. C. Howell and J. V. Breakwell, “Almost Rectilinear Halo Orbits,” *Celestial Mechanics*, Vol. 32, 1984, pp. 29–52.

[23] G. K. Nave Jr and S. D. Ross, “Global phase space structures in a model of passive descent,” *Communications in Nonlinear Science and Numerical Simulation*, Vol. 77, 2019, pp. 54–80.

[24] J. Zhong and S. D. Ross, “Differential correction and arc-length continuation applied to boundary value problems: Examples based on snap-through of circular arches,” *Applied Mathematical Modelling*, Vol. 97, 2021, pp. 81–95.

[25] J. M. Greene, R. S. MacKay, F. Vivaldi, and M. J. Feigenbaum, “Universal behaviour in families of area-preserving maps,” *Physica D: Nonlinear Phenomena*, Vol. 3, No. 3, 1981, pp. 468–486.

[26] M. Golubitsky, I. Stewart, and J. Marsden, “Generic bifurcation of Hamiltonian systems with symmetry,” *Physica D: Nonlinear Phenomena*, Vol. 24, No. 1-3, 1987, pp. 391–405.

[27] W. S. Koon, M. W. Lo, J. E. Marsden, and S. D. Ross, “Low energy transfer to the Moon,” *Celestial Mechanics and Dynamical Astronomy*, Vol. 81, 2001, pp. 63–73.

[28] M. W. Lo and S. D. Ross, “The Lunar L1 Gateway: Portal to the stars and beyond,” *AIAA Space 2001 Conference*, Albequerque, New Mexico, 2001.

[29] Z. Hasnain, C. A. Lamb, and S. D. Ross, “Capturing near-Earth asteroids around Earth,” *Acta Astronautica*, Vol. 81, No. 2, 2012, pp. 523–531.